Twisted-electron-impact single ionization of an H_2O molecule by multicenter distorted-wave calculations

Maomao Gong,[1] Yongjun Cheng,[2] Song Bin Zhang,[2,*] and Xiangjun Chen[1]

[1]*Hefei National Laboratory for Physical Sciences at Microscale and Department of Modern Physics, University of Science and Technology of China, Hefei, Anhui 230026, China*

[2]*School of Physics and Information Technology, Shaanxi Normal University, Xi'an, Shaanxi 710119, China*

(Received 30 March 2022; accepted 7 July 2022; published 22 July 2022)

We report theoretical investigation of the twisted-electron-impact single-ionization dynamics of an H_2O molecule. The triple-differential cross sections for $1b_1$, $3a_1$, $1b_2$, and $2a_1$ orbitals are obtained by a twisted-electron-impact multicenter distorted-wave method. The coplanar asymmetric kinematic condition is adopted at incident electron energy $E_i = 250$ eV and ejected electron energy $E_e = 10$ eV. By integrating the impact parameter, all possible rotation angles φ_k of the projectile are averaged for the triple-differential cross section, which is independent of the orbital angular momentum and varies as a function of opening angle θ_k. The results show that the ionization by a plane-wave projectile is more likely than by a twisted-electron projectile if the scattering angle is smaller than a critical value. However, when the scattering angle exceeds the critical point, the twisted-electron projectile can possess higher ionization probability, which will reach a maximum when the opening angle numerically approaches the scattering angle.

DOI: 10.1103/PhysRevA.106.012818

I. INTRODUCTION

Bliokh *et al.* [1] suggested that free-electron beams can carry intrinsic nonzero orbital angular momentum (OAM) in the propagation direction, called twisted- (or vortex) electron beams. Subsequently, Uchida and Tonomura [2] and Verbeeck *et al.* [3] generated the twisted-electron beams through a spiral phase plate and a versatile holographic mask in a transmission electron microscope, respectively. Then twisted-electron beams [4] with high quanta (up to $m\hbar = 100\hbar$) of OAM were produced. Since these pioneering works, research on how to generate [5,6], measure [7–9], and manipulate [10] twisted-electron beams has attracted much interest in both theory and experiment in the past decade. The extra degree of freedom for twisted-electron beams might have potential applications in nuclear and high-energy physics [11,12], atomic and molecular physics [12–14], and even nanoparticle research [15] in materials science.

Electron-impact single ionization, termed $(e, 2e)$, is one of the most fundamental processes in collision physics. The full information of the ionization dynamics can be obtained in an experiment in which the energy and momenta of the two outgoing electrons are determined, giving triple-differential cross sections (TDCSs). The $(e, 2e)$ process has been extensively studied in both theory and experiment for various kinds of atoms and molecules, for the purpose of investigating the electron-impact ionization cross section [16–19], atomic and molecular orbital imaging [20,21], molecular orientation [21,22], and radiation physics [23]. However, the complete understanding of the ionization dynamics is still one of the biggest challenges, especially for molecular targets. It originates from the difficulty resulting from the Coulomb multibody scattering states and the multicenter nature of molecules in the $(e, 2e)$ process.

Nevertheless, plenty of theoretical methods have been developed to treat the problems, including nonperturbative and perturbative methods. The nonperturbative treatments, such as the exterior complex scaling method [24], the converged close-coupling method [25], the time-dependent close-coupling method [26], and the *B*-spline *R*-matrix approach [27], have been applied to some simple atomic and molecular targets [28–30]. Basically, these kinds of *ab initio* methods can be very accurate, but do not possess high extensibility to complex molecules. On the other hand, the perturbative method, such as the distorted-wave impulse approximation [31] and distorted-wave Born approximation [31,32] for atoms and molecular three-body distorted-wave approximation [16] and multicenter (three) distorted-wave methods [18,19] for molecules, can be extended to complex molecules, but usually lack accuracy.

Theoretical investigations of the twisted-electron-impact $(e, 2e)$ process for atoms and molecules are comparatively scarce. Harris *et al.* [13] reported TDCSs for fast $(e, 2e)$ collisions with atomic hydrogen, indicating that twisted-electron ionization is less likely than a plane-wave projectile. Singh *et al.* [14] studied the TDCSs of Ar($3p$), Kr($4p$), Xe($5p$), and H_2 using the twisted distorted-wave Born approximation with impact parameter $\rho = 0$, the results showing that the TDCS is strongly influenced by the opening angle and angular momentum number of the twisted-electron projectile. A semirelativistic $(e, 2e)$ study using the Coulomb wave model with twisted-electron beams on Cu and Ag [12] was also reported.

*song-bin.zhang@snnu.edu.cn

In the present work we report a theoretical investigation of the twisted-electron-impact single-ionization process of a molecule based on multicenter distorted-wave (MCDW) theoretical calculations, called the twisted-MCDW method. The method is in the framework of the first Born approximation (FBA), which requires that the projectile electron is fast enough to be described by plane waves and the continuum wave function of an ejected electron is solved in the anisotropic multicenter potential of a molecular ion under a sudden approximation. Owing to the adopted approximations and the multicenter wave functions, the method can readily be applied to various molecules. The $(e, 2e)$ dynamics for an H_2O molecule by a twisted electron is presented in the coplanar asymmetric kinematic condition, with an incident electron energy of $E_i = 250$ eV, an ejected electron energy of $E_e = 10$ eV (8 eV if the electron is ionized from the $3a_1$ orbital), and scattering angle of $\theta_s = 15^\circ$. The cross sections for different opening angles of twisted-electron beams and different scattering angles are also analyzed in detail.

The paper is organized as follows. In the next section we briefly outline the theoretical method. The results and a discussion will be presented in Sec. III, followed by a summary in Sec. IV. Atomic units are used throughout the paper unless explicitly stated otherwise.

II. THEORETICAL METHODS

A. Bessel states of a free twisted electron

A free electron with intrinsic OAM $m\hbar$ and energy ε can be described in the cylindrical coordinates $\boldsymbol{r} = (\boldsymbol{r}_\perp, z) = (r_\perp, \varphi_r, z)$. The momentum vector of an incident electron is defined as $\boldsymbol{k}_i = (\boldsymbol{k}_{i\perp}, k_{iz}) = (k_{i\perp}, \varphi_k, k_{iz})$, which lies on the surface of a cone with an opening angle $\theta_k = \arctan(|\boldsymbol{k}_{i\perp}|/k_{iz}) = \arctan(\kappa/k_{iz})$. Here φ_k is the rotation angle. The stationary Bessel solution [11,33,34] of the field-free Schrödinger equation is

$$\langle \boldsymbol{r}|k_{iz}\kappa m\rangle = e^{ik_{iz}z}\psi_{tr}^{\kappa m}(\boldsymbol{r}_\perp) \tag{1}$$

and the transverse component of the wave function is equal to

$$\psi_{tr}^{\kappa m}(\boldsymbol{r}_\perp) = \sqrt{\kappa}\frac{e^{im\varphi_r}}{\sqrt{2\pi}}J_m(\kappa r_\perp), \tag{2}$$

where $J_m(\kappa r_\perp)$ is the mth Bessel function of the first kind. The momentum representation of the stationary Bessel solution is

$$\begin{aligned}\psi_{tr}^{\kappa m}(\boldsymbol{k}_{i\perp}) &= \frac{1}{2\pi}\int \frac{e^{im\varphi_r}}{\sqrt{2\pi}}\sqrt{\kappa}J_m(\kappa r_\perp)e^{-i\boldsymbol{k}_{i\perp}\cdot\boldsymbol{r}_\perp}d\boldsymbol{r}_\perp \\ &= (-i)^m\frac{e^{im\varphi_k}}{\sqrt{2\pi}}\frac{\delta(k_{i\perp}-\kappa)}{\sqrt{k_{i\perp}}}.\end{aligned} \tag{3}$$

Then the wave function of Eq. (1) can be written in the momentum space

$$\begin{aligned}\langle \boldsymbol{r}|k_{iz}\kappa m\rangle &= e^{ik_{iz}z}\frac{1}{2\pi}\int \psi_{tr}^{\kappa m}(\boldsymbol{k}_{i\perp})e^{i\boldsymbol{k}_{i\perp}\cdot\boldsymbol{r}_\perp}d\boldsymbol{k}_{i\perp} \\ &= (-i)^m\sqrt{\frac{\kappa}{2\pi}}\frac{1}{2\pi}\int_0^{2\pi} e^{im\varphi_k}e^{i\boldsymbol{k}_i\cdot\boldsymbol{r}}d\varphi_k.\end{aligned} \tag{4}$$

Equation (4) can be conveniently used to the subsequent transition amplitude calculation.

B. Cross section and impact parameter

According to the scattering theory [35], the eightfold-differential cross section for a given molecular orientation can be expressed as

$$\frac{d^8\sigma}{d\Omega_e d\Omega_s d\Omega dE_s} = \frac{1}{(2\pi)^5}\frac{k_e k_s}{k_{iz}}|T_{fi}(\Omega, \boldsymbol{k}_i, \boldsymbol{k}_s, \boldsymbol{k}_e)|^2, \tag{5}$$

where Ω_s and Ω_e represent the solid angles of direction for the scattered and ejected electrons, respectively; Ω represents the solid angle of molecular orientation; and $\boldsymbol{k}_i$ and E_i, $\boldsymbol{k}_s$ and E_s, and $\boldsymbol{k}_e$ and E_e are momentum vectors and energies for incident, scattering, and ejected electrons, respectively. The transition amplitude $T_{fi}(\Omega)$ gives rise to

$$\begin{aligned}&T_{fi}(\Omega, \boldsymbol{k}_i, \boldsymbol{k}_s, \boldsymbol{k}_e) \\ &\quad= \left\langle \boldsymbol{k}_s\Psi_f^{(-)}\left(\boldsymbol{k}_e; \mathcal{R}_\Omega^{-1}\{\boldsymbol{r}\}\right)|V(\{\boldsymbol{r}\})|\boldsymbol{k}_i\Psi_i\left(\mathcal{R}_\Omega^{-1}\{\boldsymbol{r}\}\right)\right\rangle.\end{aligned} \tag{6}$$

The operator $\mathcal{R}_\Omega^{-1}$ represents the rotation of the target. The scattering potential is the interaction between the projectile and molecular target, where an approximated three-body potential is employed,

$$V = \frac{1}{|\boldsymbol{r}_0 - \boldsymbol{r}_1|} - \frac{1}{N}\sum_n \frac{Z_n}{|\boldsymbol{r}_0 - \boldsymbol{R}_n|}. \tag{7}$$

Here $|\Psi_i\rangle$ is the initial bound wave function and $\{\boldsymbol{r}\}$ refers to the set of electronic coordinates. In the final state $|\Psi_f\rangle$, the ionized orbital is replaced by the continuum wave function of the ejected electron. The incident and scattered electrons are described by the plane waves $|\boldsymbol{k}_i\rangle$ and $|\boldsymbol{k}_s\rangle$. With the help of the Bethe integral

$$\int \frac{e^{i\boldsymbol{k}\cdot\boldsymbol{r}'}}{|\boldsymbol{r} - \boldsymbol{r}'|}d\boldsymbol{r}' = \frac{4\pi}{k^2}e^{i\boldsymbol{k}\cdot\boldsymbol{r}}, \tag{8}$$

the system can be simplified as a one-active-electron problem under the sudden approximation, giving rise to the expression

$$\begin{aligned}T_{fi}(\Omega, \boldsymbol{K}, \boldsymbol{k}_e) = \frac{4\pi}{K^2}&\langle \mathcal{F}^{(-)}(\boldsymbol{k}_e; \mathcal{R}^{-1}\boldsymbol{r}_e)|e^{i\boldsymbol{K}\cdot\boldsymbol{r}_e} \\ &- \frac{\sum_n Z_n e^{i\boldsymbol{K}\cdot\boldsymbol{R}_n}}{N}|\phi_\alpha(\mathcal{R}^{-1}\boldsymbol{r}_e)\rangle,\end{aligned} \tag{9}$$

where $\boldsymbol{K} = \boldsymbol{k}_i - \boldsymbol{k}_s$ is the momentum transfer; $\boldsymbol{R}_n$ is the position of the nth nucleus and Z_n indicates its charge; the vector $\boldsymbol{r}_e$ represents the position of the active electron; $|\mathcal{F}^{(-)}\rangle$ is the continuum wave function of the ejected electron; and $|\phi_\alpha\rangle$ is the bound orbital to be ionized.

In the practical experiment, the incident electron has an impact parameter $\boldsymbol{\rho}$ relative to the target, that is, the incident wave function is multiplied by a factor $e^{-i\boldsymbol{\rho}\cdot\boldsymbol{k}_i}$. Considering Eqs. (4) and (9), the transition amplitude for twisted-electron-impact single ionization with impact parameter $\boldsymbol{\rho}$ can be expressed as

$$\begin{aligned}T_{fi}^{\mathrm{tw}}(\Omega, \boldsymbol{K}, \boldsymbol{k}_e, \boldsymbol{\rho}) = (-i)^m&\sqrt{\frac{\kappa}{2\pi}}\frac{1}{2\pi} \\ &\times \int_0^{2\pi} e^{im\varphi_k - i\boldsymbol{\rho}\cdot\boldsymbol{k}_i}T_{fi}(\Omega, \boldsymbol{K}, \boldsymbol{k}_e)d\varphi_k.\end{aligned} \tag{10}$$

Integrating $|T_{fi}^{\rm tw}(\Omega, K, \boldsymbol{k}_e, \boldsymbol{\rho})|^2$ over the impact parameter $\boldsymbol{\rho}$ in the transverse plane,

$$\int d\boldsymbol{\rho}|T_{fi}^{\rm tw}(\Omega, \boldsymbol{K}, \boldsymbol{k}_e, \boldsymbol{\rho})|^2 = \frac{1}{(2\pi)^3\kappa}\int d\boldsymbol{\rho}\int e^{im\varphi_k}\delta(\kappa - k_{i\perp})T_{fi}(\Omega, \boldsymbol{K}, \boldsymbol{k}_e)e^{-i\boldsymbol{\rho}\cdot\boldsymbol{k}_{i\perp}}d\boldsymbol{k}_{i\perp} \times \int e^{-im\varphi_{k'}}\delta(\kappa - k'_{i\perp})T_{fi}^{*}(\Omega, \boldsymbol{K}', \boldsymbol{k}_e)e^{i\boldsymbol{\rho}\cdot\boldsymbol{k}'_{i\perp}}d\boldsymbol{k}'_{i\perp}, \quad (11)$$

with the help of the integral

$$\int d^2\rho\, e^{i\boldsymbol{\rho}\cdot(\boldsymbol{p}''-\boldsymbol{p}')} = (2\pi)^2\delta_2(\boldsymbol{p}'_\perp - \boldsymbol{p}''_\perp), \quad (12)$$

Eq. (11) can be simplified by integrating $d\boldsymbol{\rho}$ and $d\boldsymbol{k}'_{i\perp}$,

$$\int d\boldsymbol{\rho}|T_{fi}^{\rm tw}(\Omega, \boldsymbol{K}, \boldsymbol{k}_e, \boldsymbol{\rho})|^2 = \frac{1}{2\pi\kappa}\int |\delta(\kappa - k_{i\perp}) \times T_{fi}(\Omega, \boldsymbol{K}, \boldsymbol{k}_e)|^2 d\boldsymbol{k}_{i\perp}. \quad (13)$$

Using the expression of the δ function squared from [11] and performing the integration over $k_{i\perp}$, the eightfold differential cross section for the twisted-electron-impact single-ionization process finally yields

$$\frac{d^8\sigma(\mathcal{T})}{d\Omega_e d\Omega_s d\Omega dE_s} = \frac{1}{2\pi\cos\theta_k}\frac{1}{(2\pi)^5}\frac{k_e k_s}{k_i} \times \int |T_{fi}(\Omega, \boldsymbol{K}, \boldsymbol{k}_e)|^2 d\varphi_k. \quad (14)$$

By averaging over all molecular orientations, the fivefold differential cross section, or commonly termed TDCS, is obtained:

$$\frac{d^5\sigma(\mathcal{T})}{d\Omega_e d\Omega_s dE_s} = \frac{1}{2\pi\cos\theta_k}\frac{1}{(2\pi)^5}\frac{k_e k_s}{k_i}\frac{1}{8\pi^2} \times \iint |T_{fi}(\Omega, \boldsymbol{K}, \boldsymbol{k}_e)|^2 d\Omega d\varphi_k. \quad (15)$$

The magnitude of momentum transfer is given by $K^2 = k_i^2 + k_s^2 - 2k_i k_s\cos\theta$, where $\cos\theta = \cos\theta_k\cos\theta_s + \sin\theta_k\sin\theta_s\cos(\varphi_k - \varphi_s)$. The cross section of the twisted-electron-impact ionization process by integrating the impact parameters does not depend on the magnitude of the angular momentum of the projectile. Equation (15) is a classic expression as the TDCS of twisted-electron-impact single ionization is simply obtained by averaging over all directions of $\boldsymbol{k}_i$ along the cone surface.

C. Multicenter distorted waves

In the single-ionization process, the active bound electron is assumed to be ionized to the continuum orbital. Then the ejected electron is regarded as moving in the anisotropic residual ion potential under a sudden approximation, while the scattering electron is too fast to affect the motion of the ejected electron. In order to obtain an accurate continuum wave function of the ejected electron, a model potential [18] is adopted to include the response of bound electrons and the exchange effect

$$V^m = V^{\rm st} + V^{\rm CP} + V^{\rm model\ exc}, \quad (16)$$

where $V^{\rm st}$ is the electrostatic potential between the incident electron and the residual molecular ion and $V^{\rm CP}$ and $V^{\rm model\ exc}$ are the correlation-polarization potential and the model exchange potential, respectively.

The continuum wave function of the ejected electron $\mathcal{F}^{(-)}$ in Eq. (9) is obtained by solving the effective Schrödinger equation

$$\left(-\tfrac{1}{2}\nabla^2 + V^m - E_{k_e}\right)\mathcal{F}^{(-)}(\boldsymbol{k}_e; \boldsymbol{r}_e) = 0. \quad (17)$$

The anisotropic multicenter feature of $\mathcal{F}^{(-)}(\boldsymbol{k}_e; \boldsymbol{r}_e)$ is inherited from V^m. To solve this equation, the single-centered expansion technique [36–38] is employed, where the wave function and potential are expanded over the symmetry-adapted angular functions [36–38]. It should note that the model potential V^m is anisotropic and introduces couplings between terms of different angular momentum in the partial wave expansion of $\mathcal{F}^{(-)}(\boldsymbol{k}_e; \boldsymbol{r}_e)$, resulting in a set of coupled equations. As shown in our previous work [18], the diagonal terms in the potential matrix are considered dominant. Thus, in practical calculation, we will ignore the off-diagonal elements and solve the decoupled partial wave equations.

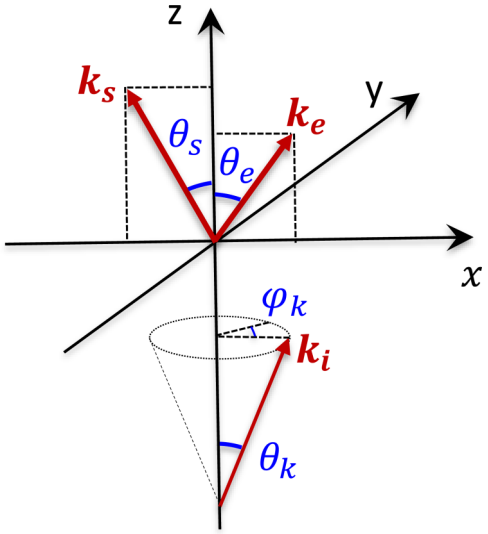

FIG. 1. Coordinate system in the present calculations.

D. Details of calculation

The H_2O molecule belongs to the C_{2V} point group and its ground electronic configuration is $(1a_1)^2(2a_1)^2(1b_2)^2(3a_1)^2(1b_1)^2$ with bond length $R_{\rm O\text{-}H} = 1.81$ a.u. and bond angle $\angle_{\rm H\text{-}O\text{-}H} = 104.5^\circ$. It is a typical candidate for theoretical investigations, as it has been studied by various theoretical models [39,40]. Experimental date for $(e, 2e)$ by twisted-electron impact on an H_2O molecule are lacking; theoretical research to show the different physics is needed. In the present work we choose kinematic conditions adopted by Milne-Brownlie *et al.* [45]

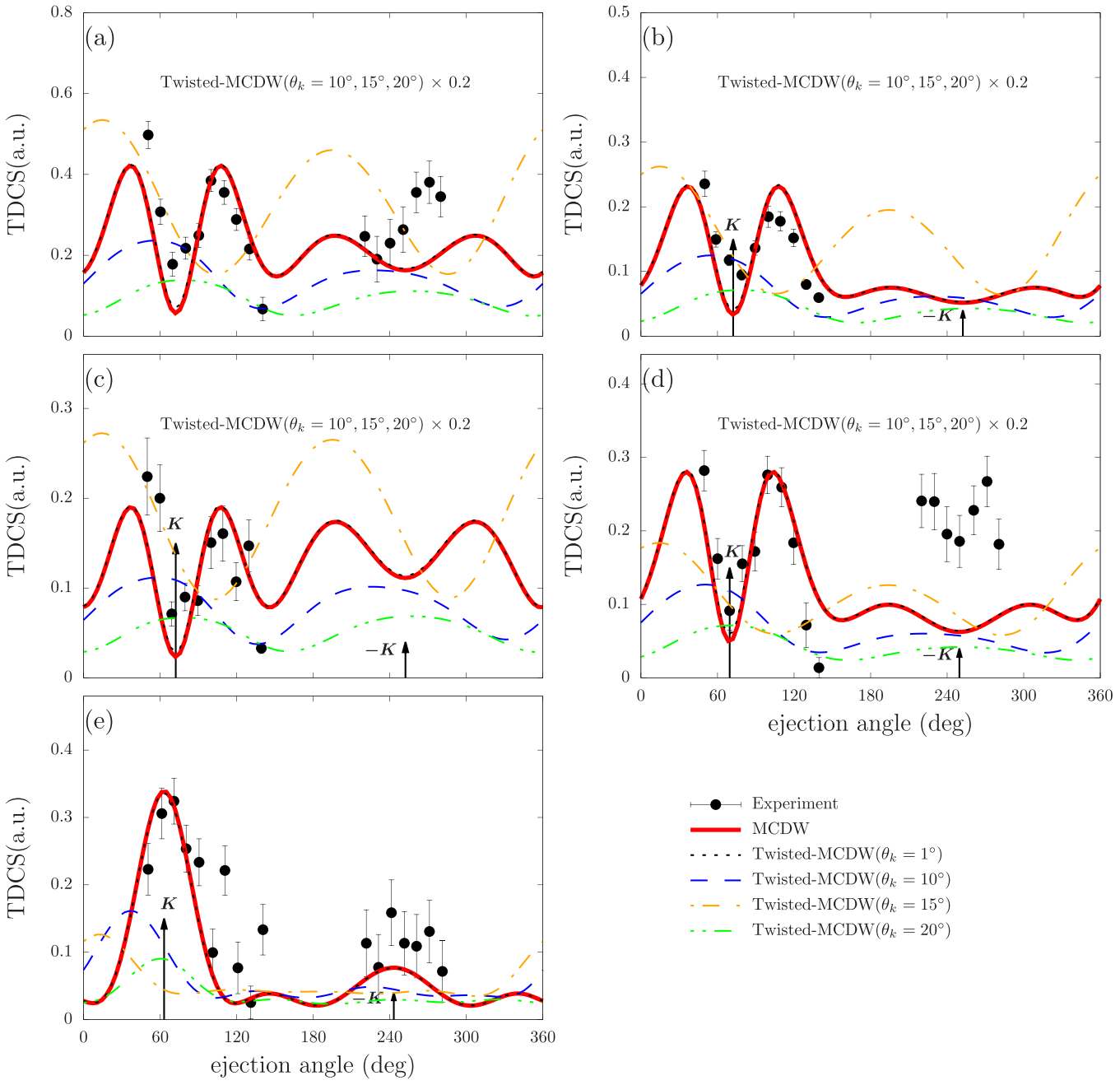

FIG. 2. TDCSs of a H_2O molecule for different orbitals: (a) $1b_1 + 3a_1$, (b) $1b_1$, (c) $3a_1$, (d) $1b_2$, and (e) $2a_1$. The incident electron energy E_i is 250 eV, the ejected electron energy E_e is 10 eV (8 eV if the electron is ionized from the $3a_1$ orbital), and the scattering angle is 15°. The experimental data (closed circles) are taken from [45]. The red solid line represents the MCDW calculation, while dotted lines are twisted-MCDW calculations for different opening angles of the twisted-electron beams.

to study the single-ionization process. The experiments were performed under coplanar asymmetric geometry at an incident electron energy of $E_i = 250$ eV, an ejected electron energy of $E_e = 10$ eV (8 eV for ionization from the $3a_1$ orbital), and a scattering angle of $\theta_s = 15°$.

The bound wave functions of molecular orbitals (MOs) are calculated using the GAUSSIAN 09 [41] program with density-functional theory employing a B3LYP hybrid functional [42,43] and cc-pVTZ basis set [44]. Then the MOs are expanded over symmetry-adapted angular functions. Let l_{bmax} and l_{cmax} denote the upper limits of angular momenta in the partial-wave expansions for bound orbital and continuum wave functions, respectively. In the present calculations, convergence of TDCSs is achieved with $l_{\text{bmax}} = 10$ and $l_{\text{cmax}} = 18$. In the single-center expansion, r ranges from 0 to 8.47 a.u. with increasing step size from 0.01 to 0.128 a.u. The numerical spherical average of the Euler angle mesh $N_\alpha = N_\beta = N_\gamma = 12$, where N_α, N_β, and N_γ represent the number of points for Euler angles α, β, and γ, respectively. Figure 1 shows the coordinate system in the present calculations. The twisted-electron projectile propagates along the z axis, with the scattering electron momentum vector being fixed at

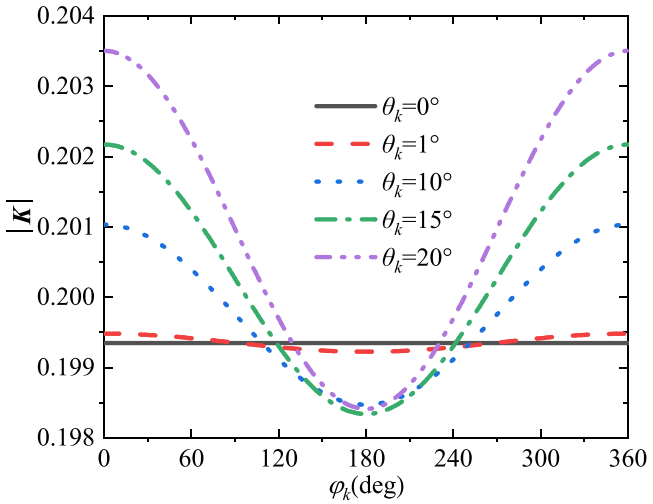

FIG. 3. Magnitude of the electron momentum transfer vector $|\boldsymbol{K}|$ as a function of φ_k for different opening angles of the twisted-electron projectile θ_k.

$\theta_s = 15^\circ$ and $\varphi_s = 180^\circ$ and the ejected electron lying in the xz plane. For the twisted-electron impact, it is actually not a strict coplanar geometry, as the twisted electron possesses OAM in the transverse plane. Here we still use the terminology as in the conventional $(e, 2e)$. Note that the present method has been used to check the calculations for the ionization of atomic hydrogen and it generates the same results obtained by Harris *et al.* [13].

III. RESULTS AND DISCUSSION

Figure 2 shows the TDCSs of $1b_1$, $3a_1$, $1b_2$, and $2a_1$ orbitals as a function of ejection angle θ_e. The red solid lines represent the result of the MCDW method or the twisted-MCDW calculation with an opening angle of $\theta_k = 0^\circ$. The closed circles represent the experimental data, reported by Milne-Brownlie *et al.* [45] using a conventional electron beam, and can be reasonably reproduced by the present MCDW calculations, indicating the validity of present model. The binary region, approximated between $\theta_e = 0^\circ$ and $\theta_e = 180^\circ$, represents the binary collision between incident and active bound electrons. The recoil region, which is approximately the opposite direction of the momentum transfer vector, is usually regarded as the backward reflection of an ejected electron by the residual ion potential. Actually, the MCDW method is not capable of completely reproducing the experimental data at $E_i = 250$ eV; the FBA approximately holds at the impact energy. In Figs. 2(a)–2(d) the double-peak structure in the binary region reflects the p character of $1b_1$, $3a_1$, and $1b_2$ orbitals and is well described by the MCDW method. In the recoil region, the MCDW method fails to reproduce the distribution of experimental data. In Fig. 2(e), for the ionization of a typical s-type $2a_1$ orbital, the single binary and recoil peaks are both well described by MCDW calculations.

It has been well established that the traditional $(e, 2e)$ experiment does not measure the impact parameter. In the practical calculation, it is necessary to average over all impact parameters. Unfortunately, that means a loss of information on OAM and only leaves the dependence of the opening angle of the projectile, as Eq. (15) shows. In order to investigate the effect of twisted-electron beams on the cross sections, four nonzero opening angles ($\theta_k = 1^\circ$, 10°, 15°, and 20°) are considered in the twisted-MCDW calculations, as shown by the dotted lines in Fig. 2. The calculation at $\theta_k = 1^\circ$ is nearly the same as the MCDW result, while calculations for $\theta_k = 10^\circ$, 15°, and 20° are largely different from the MCDW results. Note that in Figs. 2(a)–2(d), the calculated TDCSs at $\theta_k = 10^\circ$, 15°, and 20° have multiplied by a factor 0.2. For the s-type $2a_1$ orbital, there is no additional factor to be multiplied in Fig. 2(e). Obviously, the twisted-electron-impact single ionization is more likely than the plane-wave projectile for p-type $1b_1$, $3a_1$, and $1b_2$ orbitals and less likely for the s-type $2a_1$ orbital, which is partially different from the conclusions of Harris *et al.* [13] when investigating the ionization of atomic hydrogen.

Equation (15) tells us that the difference between twisted-MCDW and MCDW calculations mainly comes from the different momentum transfer for the integration of φ_k. As stated before, the magnitude of the momentum transfer is given by $K^2 = k_i^2 + k_s^2 - 2k_i k_s \cos\theta$, with $\cos\theta = \cos\theta_k \cos\theta_s + \sin\theta_k \sin\theta_s \cos(\varphi_k - \varphi_s)$. In the present calculations, $\varphi_s = 180^\circ$, for a fixed value of θ_k, and the magnitude of the momentum transfer will be a minimum when $\varphi_k = 180^\circ$. Figure 3 plots the magnitude of the momentum transfer as a function of φ_k for five opening angles of a twisted-electron projectile. There $\theta_k = 0^\circ$ corresponds to a plane-wave electron beam and $|\boldsymbol{K}|$ is a constant. With the increase of θ_k ($\theta_k = 1^\circ$, 10°, 15°, and 20°), it becomes a more concave shape symmetrical about $\varphi_k = 180^\circ$. The term $1/K^4$ in Eq. (15) will affect the TDCS distribution to concentrate around $\varphi_k = 180^\circ$. The effect is further enhanced by the $\boldsymbol{K}$-related integration over $\boldsymbol{r}_e$ in Eq. (9) and will be illustrated later.

To gain deeper insight into the twisted-electron-impact cross sections, for the $1b_1$ orbital, the two-dimensional (2D) density images of TDCSs as functions of φ_k and θ_e for $\theta_k = 0^\circ$, 1°, 10°, 15°, and 20° are displayed in Fig. 4. In Fig. 4(a), for the non-twisted-electron beam, the distribution of the TDCS as a function of φ_k and θ_k will not change with the increase of φ_k. From $\theta_k = 1^\circ$ to 20°, the TDCS distribution gradually concentrates around $\varphi_k = 180^\circ$. In the coplanar asymmetric kinematic condition, the TDCS has a preferred twisted-electron momentum direction of $\varphi_k = 180^\circ$, which is determined by the magnitude of the momentum transfer vector. It is worth noting that Fig. 4(d) corresponds to $\theta_k = \theta_s = 15^\circ$, which means that a global minimum of $|\boldsymbol{K}|$ exists under the kinematic condition. It can be simply proved by the minimum of the green dash-dotted line in Fig. 3. The distribution of the TDCS in the θ_e dimension also changes dramatically for different θ_k, which also results from the variation of momentum transfer for the twisted-electron-impact scattering process.

Since the $1b_1$, $3a_1$, and $1b_2$ orbitals behave as similar p-type characters, we choose $1b_1$ and $2a_1$ orbitals for the subsequent analysis. Figure 5 shows the 2D density maps by integrating TDCSs over θ_e in the coplanar geometry as functions of the twisted-electron projectile parameters θ_k and φ_k. In Fig. 5(a), the cross section for the $1b_1$ orbital around

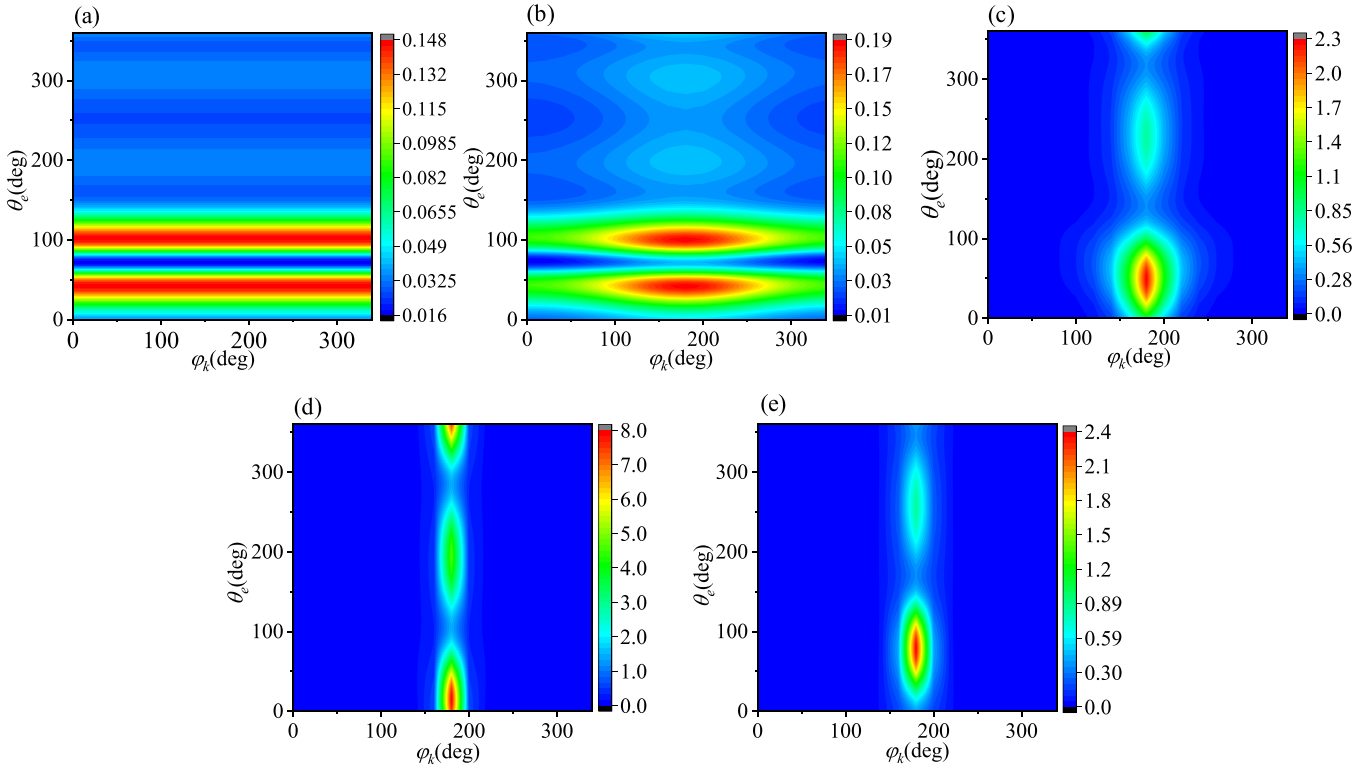

FIG. 4. The 2D density maps of TDCSs as functions of φ_k and θ_e for the $1b_1$ orbital in Fig. 2(b): (a) $\theta_k = 0^\circ$, (b) $\theta_k = 1^\circ$, (c) $\theta_k = 10^\circ$, (d) $\theta_k = 15^\circ$, and (e) $\theta_k = 20^\circ$.

$\theta_k = 15^\circ$ and $\varphi_k = 180^\circ$ is more intense than other areas. Also, the preferred twisted-electron momentum direction is $\varphi_k = 180^\circ$, as mentioned before, but it will be slightly different for the $2a_1$ orbital in Fig. 5(b). The full width at half maximum of the cross section for each θ_k gradually decreases with the increase of θ_k. Unlike the $1b_1$ orbital, if we integrate φ_k as in Eq. (15), $\theta_k = 0^\circ$ will give rise to the largest absolute cross section. It should be noted that the absolute TDCSs at $\theta_k = 10^\circ$, 15°, and 20° for twisted-MCDW calculations have been multiplied by 0.2 in Figs. 2(a)–2(d), while the factor is 1.0 for the $2a_1$ orbital, as shown in Fig. 2(e). This is consistent with the results in Fig. 5. The twisted-electron-impact single ionization yields different characters for *p*-type and *s*-type orbitals of H_2O for the kinematic condition of $E_i = 250$ eV, $E_e = 10$ eV, and $\theta_s = 15^\circ$. The twisted-electron-impact ionization by averaging over all φ_k for the *p*-type $1b_1$ orbital is more likely to happen than a plane-wave projectile if θ_k numerically approaches θ_s for the present kinematic condition and less likely for the *s*-type $2a_1$ orbital.

The important different feature of $1b_1$ and $2a_1$ orbitals shows the complicated dynamics of twisted-electron-impact ionization of molecules. A possible way to understand the process is to see what will happen to the cross section for various kinematic conditions. We know that the projectile scattering angle is directly related to the momentum transfer vector. Here we intend to change the projectile scattering angle while keep other kinematic parameters fixed. Figure 6 shows the 2D density maps of cross sections by integrating φ_k and θ_e in the coplanar geometry at $E_i = 250$ eV and $E_e = 10$ eV as functions of θ_k and θ_s for $1b_1$ and $2a_1$ orbitals. In Fig. 6(a), the cross section is mainly centered around the line $\theta_s = \theta_k$. In other words, the cross section is more intense when $\theta_k = \theta_s$. However, if θ_s is smaller than a critical angle of about 6°, the cross sections for $\theta_k = 0^\circ$ show the maximum intensity. The situation is quite different for the $2a_1$ orbital, as indicated in Fig. 6(b). The $2a_1$ orbital has a larger critical scattering angle of about 18°. So the different characters between $1b_1$ and $2a_1$ orbitals at $\theta_s = 15^\circ$ in Figs. 2 and 5 are directly explained. As the twisted-electron projectile is described by the plane wave in the present method, it is reasonably to doubt that the multicenter distorted wave of an ejected electron is responsible for the important different feature for $1b_1$ and $2a_1$ orbitals. Our further test calculations show that the Coulomb wave description displays similar results to the above exploration. This indicates that the different characters from twisted-electron impact are strongly related to the shape of the ionized orbital. We believe that in the twisted-electron scattering experiment, the extra degree of freedom for the twisted projectile is not the only excuse to introduce new physics; additional different kinematic conditions and targets are highly desired for future exploration.

IV. SUMMARY

We have reported a theoretical study of the twisted-electron-impact single-ionization dynamics of an H_2O molecule for the traditional $(e, 2e)$ experimental condition. The TDCSs of $1b_1$, $3a_1$, $1b_2$, and $2a_1$ orbitals are obtained by the twisted-MCDW method in the coplanar geometry at $E_i = 250$ eV, $E_e = 10$ eV, and $\theta_s = 15^\circ$. The TDCS varies as

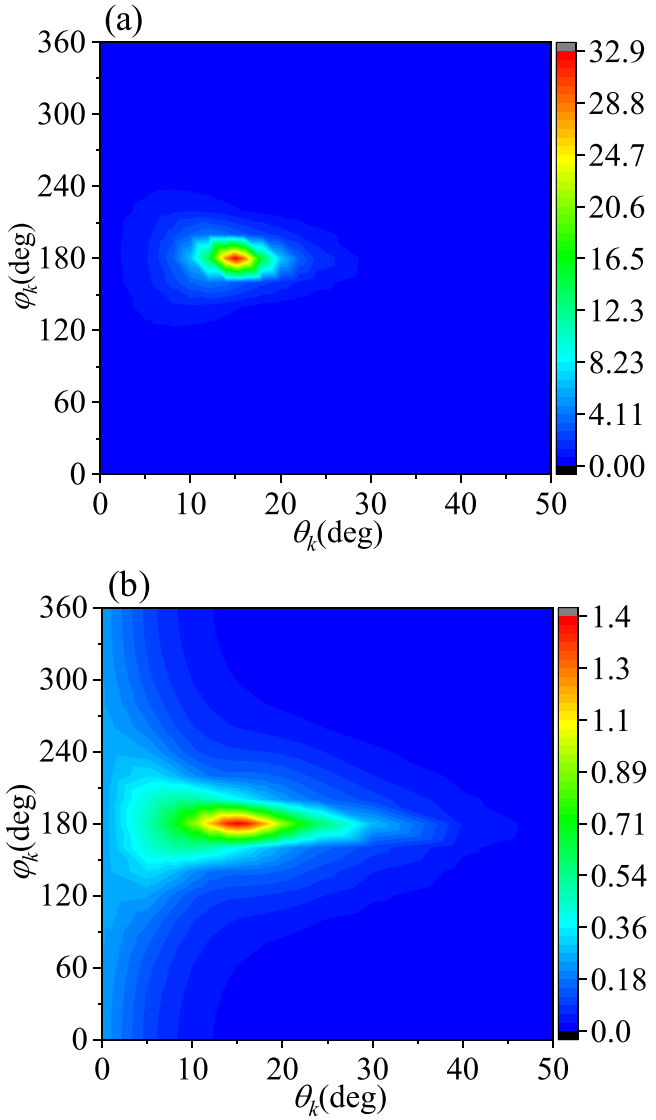

FIG. 5. The 2D density maps of TDCSs by integrating θ_e in the coplanar kinematics as functions of the twisted-electron projectile parameters θ_k and φ_k for orbitals (a) $1b_1$ and (b) $2a_1$.

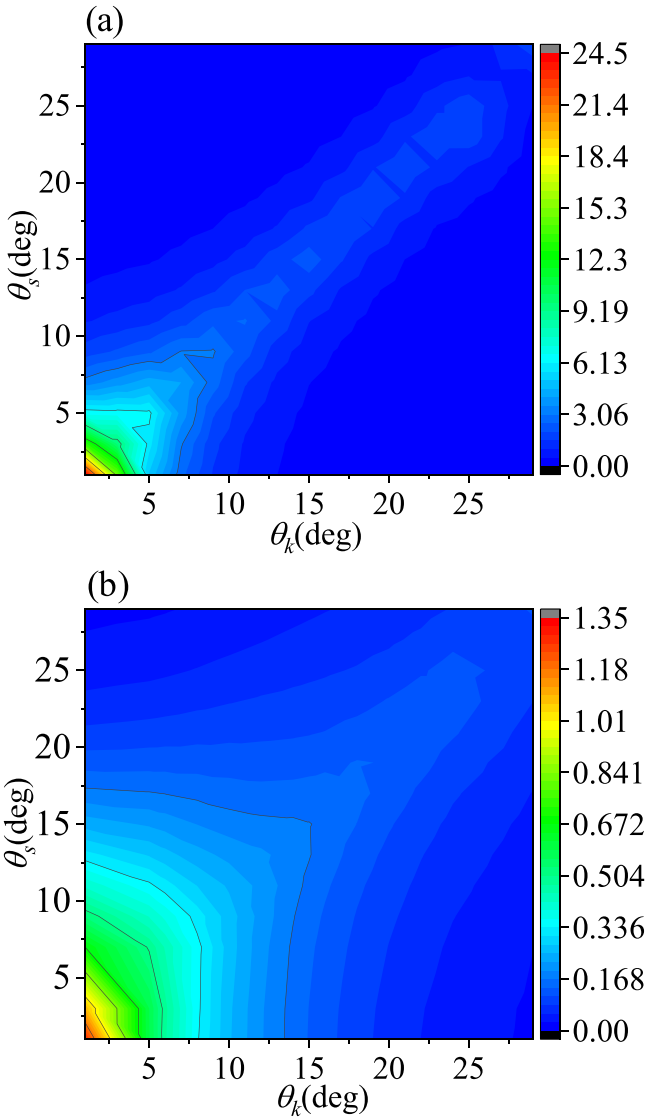

FIG. 6. The 2D density maps of cross sections by integrating φ_k and θ_e in the coplanar kinematics as functions of θ_k and θ_s for orbitals (a) $1b_1$ and (b) $2a_1$.

a function of opening angle θ_k by averaging over all possible rotation angles φ_k of the projectile and does not depend on the orbital angular momentum. The twisted-MCDW calculations successfully reproduced the TDCSs of the MCDW model for $\theta_k = 0°$, suggesting the validity of the present model. The cross sections for different θ_k and φ_k show that the TDCS is more intense around $\theta_k = \theta_s$ and $\varphi_k = 180°$. The twisted-electron-impact ionization for $1b_1$, $3a_1$, and $1b_2$ orbitals is more likely to happen than a plane-wave projectile for the present kinematic condition, while it is the opposite for the $2a_1$ orbital.

The cross sections of $1b_1$ and $2a_1$ orbitals for scattering angles ranging from 0° to 30° have also been investigated. The $1b_1$ and $2a_1$ orbitals have critical scattering angles of about 6° and 18°, respectively. The ionization by the plane-wave projectile is more likely than by a twisted-electron projectile if the scattering angle is smaller than a critical value. However, when the scattering angle exceeds the critical point, the twisted-electron projectile can possess higher ionization probability, which will reach a maximum when the opening angle of the projectile numerically approaches the scattering angle. The results indicate that, for different types of orbitals, the twisted-electron-impact cross section exhibits quite different character. The present work has clearly presented the very different and complicated dynamics induced by twisted electron; further, more in-depth investigation of different kinematics and targets are required to reveal the underlying dynamics.

ACKNOWLEDGMENTS

Grants from the National Natural Science Foundation of China (No. 12004370, No. 11534011, No. 11934004, and No. 11974230) are acknowledged.

[1] K. Y. Bliokh, Y. P. Bliokh, S. Savel'ev, and F. Nori, Phys. Rev. Lett. **99**, 190404 (2007).

[2] M. Uchida and A. Tonomura, Nature (London) **464**, 737 (2010).

[3] J. Verbeeck, H. Tian, and P. Schattschneider, Nature (London) **467**, 301 (2010).

[4] B. J. McMorran, A. Agrawal, I. M. Anderson, A. A. Herzing, H. J. Lezec, J. J. McClelland, and J. Unguris, Science **331**, 192 (2011).

[5] N. Voloch-Bloch, Y. Lereah, Y. Lilach, A. Gover, and A. Arie, Nature (London) **494**, 331 (2013).

[6] V. Grillo, G. C. Gazzadi, E. Mafakheri, S. Frabboni, E. Karimi, and R. W. Boyd, Phys. Rev. Lett. **114**, 034801 (2015).

[7] K. Saitoh, Y. Hasegawa, K. Hirakawa, N. Tanaka, and M. Uchida, Phys. Rev. Lett. **111**, 074801 (2013).

[8] G. Guzzinati, L. Clark, A. Béché, and J. Verbeeck, Phys. Rev. A **89**, 025803 (2014).

[9] V. Grillo, A. H. Tavabi, F. Venturi, H. Larocque, R. Balboni, G. C. Gazzadi, S. Frabboni, P.-H. Lu, E. Mafakheri, F. Bouchard, R. E. Dunin-Borkowski, R. W. Boyd, M. P. J. Lavery, M. J. Padgett, and E. Karimi, Nat. Commun. **8**, 15536 (2017).

[10] A. J. Silenko, P. Zhang, and L. Zou, Phys. Rev. Lett. **119**, 243903 (2017).

[11] V. Serbo, I. P. Ivanov, S. Fritzsche, D. Seipt, and A. Surzhykov, Phys. Rev. A **92**, 012705 (2015).

[12] A. Mandal, N. Dhankhar, D. Sébilleau, and R. Choubisa, Phys. Rev. A **104**, 052818 (2021).

[13] A. L. Harris, A. Plumadore, and Z. Smozhanyk, J. Phys. B **52**, 094001 (2019).

[14] P. Singh, C. Champion, and R. K. Sharma, J. Phys. B **54**, 195202 (2021).

[15] J. Verbeeck, P. Schattschneider, S. Lazar, M. Stöger-Pollach, S. Löffler, A. Steiger-Thirsfeld, and G. Van Tendeloo, Appl. Phys. Lett. **99**, 203109 (2011).

[16] D. H. Madison and O. Al-Hagan, J. At. Mol. Opt. Phys. **2010**, 367180 (2010).

[17] I. Bray, D. Fursa, A. Kadyrov, A. Stelbovics, A. Kheifets, and A. Mukhamedzhanov, Phys. Rep. **520**, 135 (2012).

[18] S. B. Zhang, X. Y. Li, J. G. Wang, Y. Z. Qu, and X. Chen, Phys. Rev. A **89**, 052711 (2014).

[19] M. Gong, X. Li, S. B. Zhang, S. Niu, X. Ren, E. Wang, A. Dorn, and X. Chen, Phys. Rev. A **98**, 042710 (2018).

[20] M. Takahashi, Bull. Chem. Soc. Jpn. **82**, 751 (2009).

[21] M. Takahashi, N. Watanabe, Y. Khajuria, Y. Udagawa, and J. H. D. Eland, Phys. Rev. Lett. **94**, 213202 (2005).

[22] S. Bellm, J. Lower, E. Weigold, and D. W. Mueller, Phys. Rev. Lett. **104**, 023202 (2010).

[23] I. Baccarelli, I. Bald, F. A. Gianturco, E. Illenberger, and J. Kopyra, Phys. Rep. **508**, 1 (2011).

[24] J. Colgan, O. Al-Hagan, D. H. Madison, C. Kaiser, A. J. Murray, and M. S. Pindzola, Phys. Rev. A **79**, 052704 (2009).

[25] I. Bray and A. T. Stelbovics, Phys. Rev. A **46**, 6995 (1992).

[26] M. S. Pindzola, F. Robicheaux, S. D. Loch, J. C. Berengut, T. Topcu, J. Colgan, M. Foster, D. C. Griffin, C. P. Ballance, D. R. Schultz, T. Minami, N. R. Badnell, M. C. Witthoeft, D. R. Plante, D. M. Mitnik, J. A. Ludlow, and U. Kleiman, J. Phys. B **40**, R39 (2007).

[27] O. Zatsarinny and K. Bartschat, Phys. Rev. A **85**, 062709 (2012).

[28] J. Colgan, M. S. Pindzola, F. Robicheaux, C. Kaiser, A. J. Murray, and D. H. Madison, Phys. Rev. Lett. **101**, 233201 (2008).

[29] M. S. Pindzola, S. A. Abdel-Naby, J. A. Ludlow, F. Robicheaux, and J. Colgan, Phys. Rev. A **85**, 012704 (2012).

[30] M. C. Zammit, D. V. Fursa, and I. Bray, Phys. Rev. A **87**, 020701(R) (2013).

[31] I. McCarthy, Aust. J. Phys. **48**, 1 (1995).

[32] D. H. Madison, R. V. Calhoun, and W. N. Shelton, Phys. Rev. A **16**, 552 (1977).

[33] I. P. Ivanov and V. G. Serbo, Phys. Rev. A **84**, 033804 (2011).

[34] D. V. Karlovets, G. L. Kotkin, V. G. Serbo, and A. Surzhykov, Phys. Rev. A **95**, 032703 (2017).

[35] J. R. Taylor, *Scattering Theory: The Quantum Theory of Non-relativistic Collisions* (Courier, Chelmsford, 2006).

[36] N. Sanna and F. Gianturco, Comput. Phys. Commun. **128**, 139 (2000).

[37] N. Sanna and G. Morelli, Comput. Phys. Commun. **162**, 51 (2004).

[38] N. Sanna, I. Baccarelli, and G. Morelli, Comput. Phys. Commun. **180**, 2544 (2009).

[39] C. Champion, C. Dal Cappello, S. Houamer, and A. Mansouri, Phys. Rev. A **73**, 012717 (2006).

[40] C.-Y. Lin, C. W. McCurdy, and T. N. Rescigno, Phys. Rev. A **89**, 012703 (2014).

[41] M. J. Frisch, G. W. Trucks, H. B. Schlegel, G. E. Scuseria, M. A. Robb, J. R. Cheeseman, G. Scalmani, V. Barone, B. Mennucci, G. A. Petersson, H. Nakatsuji, M. Caricato, X. Li, H. P. Hratchian, A. F. Izmaylov, J. Bloino, G. Zheng, J. L. Sonnenberg, M. Hada, M. Ehara *et al.*, Gaussian 09 Revision A.02 is the program being used in the present work.

[42] A. D. Becke, J. Chem. Phys. **98**, 5648 (1993).

[43] C. Lee, W. Yang, and R. G. Parr, Phys. Rev. B **37**, 785 (1988).

[44] T. H. Dunning Jr., J. Chem. Phys. **90**, 1007 (1989).

[45] D. S. Milne-Brownlie, S. J. Cavanagh, B. Lohmann, C. Champion, P. A. Hervieux, and J. Hanssen, Phys. Rev. A **69**, 032701 (2004).